THE JOURNAL OF PHYSICAL CHEMISTRY B

Article

pubs.acs.org/JPCB

Small-Angle X-ray Scattering Insights into the Architecture-Dependent Emulsifying Properties of Amphiphilic Copolymers in Supercritical Carbon Dioxide

David Alaimo,[†] Daniel Hermida Merino,[‡] Bruno Grignard,[†] Wim Bras,[‡] Christine Jérôme,[†] Antoine Debuigne,*[,†] and Cedric J. Gommes*[,§,∥]

[†]Center for Education and Research on Macromolecules (CERM), University of Liège, B6a, Sart-Tilman, B-4000 Liège, Belgium

[‡]DUBBLE@ESRF, Netherlands Organization for Scientific Research (NWO), 6 Rue Jules Horowitz, Grenoble 38043, France

[§]Department of Chemical Engineering, University of Liège, B6a, Sart-Tilman, B-4000 Liège, Belgium

[∥]Polymer Chemistry and Materials, Chemistry Department, Katholieke Universiteit Leuven, Celestijnenlaan 200F, B-3001 Leuven, Belgium

Supporting Information

ABSTRACT: The supramolecular assembly of a series of copolymers combining poly(ethylene oxide)-rich hydrophilic and fluorinated CO_2-philic sequences is analyzed by synchrotron small-angle X-ray scattering (SAXS) in supercritical CO_2, as well as in water/CO_2 emulsions. These copolymers were designed to have the same molecular weight and composition and to differ only by their macromolecular architecture. The investigated copolymers have random, block, and palm-tree architectures. Besides, thermoresponsive copolymer is also analyzed, having a hydrophilic sequence becoming water-insoluble around 41 °C, i.e., just above the critical point of CO_2. At the length scale investigated by SAXS, only the random copolymer appears to self-assemble in pure CO_2, in the form of a disordered microgel-like network. The random, block, and thermoresponsive copolymers are all able to stabilize water/CO_2 emulsions but not the copolymer with the palm-tree architecture, pointing at the importance of macromolecular architecture for the emulsifying properties. A modeling of the SAXS data shows that the block and the thermoresponsive copolymers form spherical micelle-like structures containing about 70% water and 30% polymer.

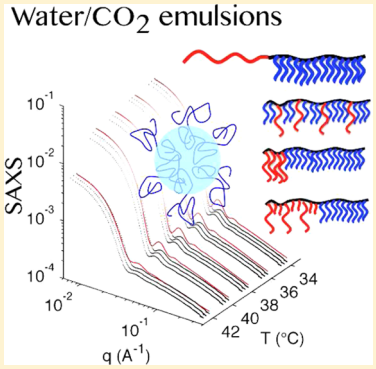

1. INTRODUCTION

Supercritical fluids have received increasing attention over the past decades as alternatives to organic solvents traditionally used in many areas including extraction processes,[1,2] organic chemistry,[3] and polymer synthesis.[4] Supercritical carbon dioxide ($scCO_2$) is particularly suitable for those applications because it is inexpensive, nonflammable, nontoxic and environmentally benign, and its critical parameters, under which processing can take place, are easily reached (73.8 bar and 31.1 °C). Moreover, the viscosity, density, and solvation power of this fluid can be tuned over a large scale by simple adjustment of pressure and temperature. The main limitation of $scCO_2$ is its poor ability to solubilize polar species and macromolecules, which notably includes proteins and almost all synthetic polymers. Notable exceptions are low-molar-mass poly(vinyl esters),[5] polysiloxanes[6] and particularly perfluorinated copolymers[7−9] which are well-soluble in CO_2. This explains the increasing use of the latter molecules in CO_2 as stabilizers for particles synthesis,[7,9−11] emulsion stabilization,[12,13] as well as metal complexation and extraction.[14,15]

Polymers with stabilizing properties in CO_2 all consist of CO_2-philic and CO_2-phobic parts.[9,16,17] It was found that the composition and molar mass of the macromolecules strongly affect their performance in applications.[18,19] For example, the size of poly(methyl methacrylate) (PMMA) polymer particles prepared by dispersion polymerization in $scCO_2$[19] proved to be dependent on the nature and the structure of the stabilizer as well as the diameter of water droplets in water/CO_2 emulsion[18] stabilized with fluorinated copolymers. A wide variety of polymer stabilizers is described in the literature,[5,7,17,20] notably in the context of studies on heterogeneous systems such as emulsions[18] and dispersions,[9,21] with possible architectures including block[7] and random[22] copolymers. However, the relation between the structural characteristics of the stabilizer and their performances in $scCO_2$ remain poorly understood.

Small-angle X-ray scattering (SAXS) is a suitable experimental tool to gain insights into supramolecular assemblies. It enables one to study submicronic objects formed by (macro)molecules in $scCO_2$, and especially their tendency to form micelles or colloids in aqueous dispersed media.[22−30] Although

Received: August 27, 2014
Revised: November 11, 2014
Published: December 16, 2014

DOI: 10.1021/jp5086558
J. Phys. Chem. B 2015, 119, 1706−1716

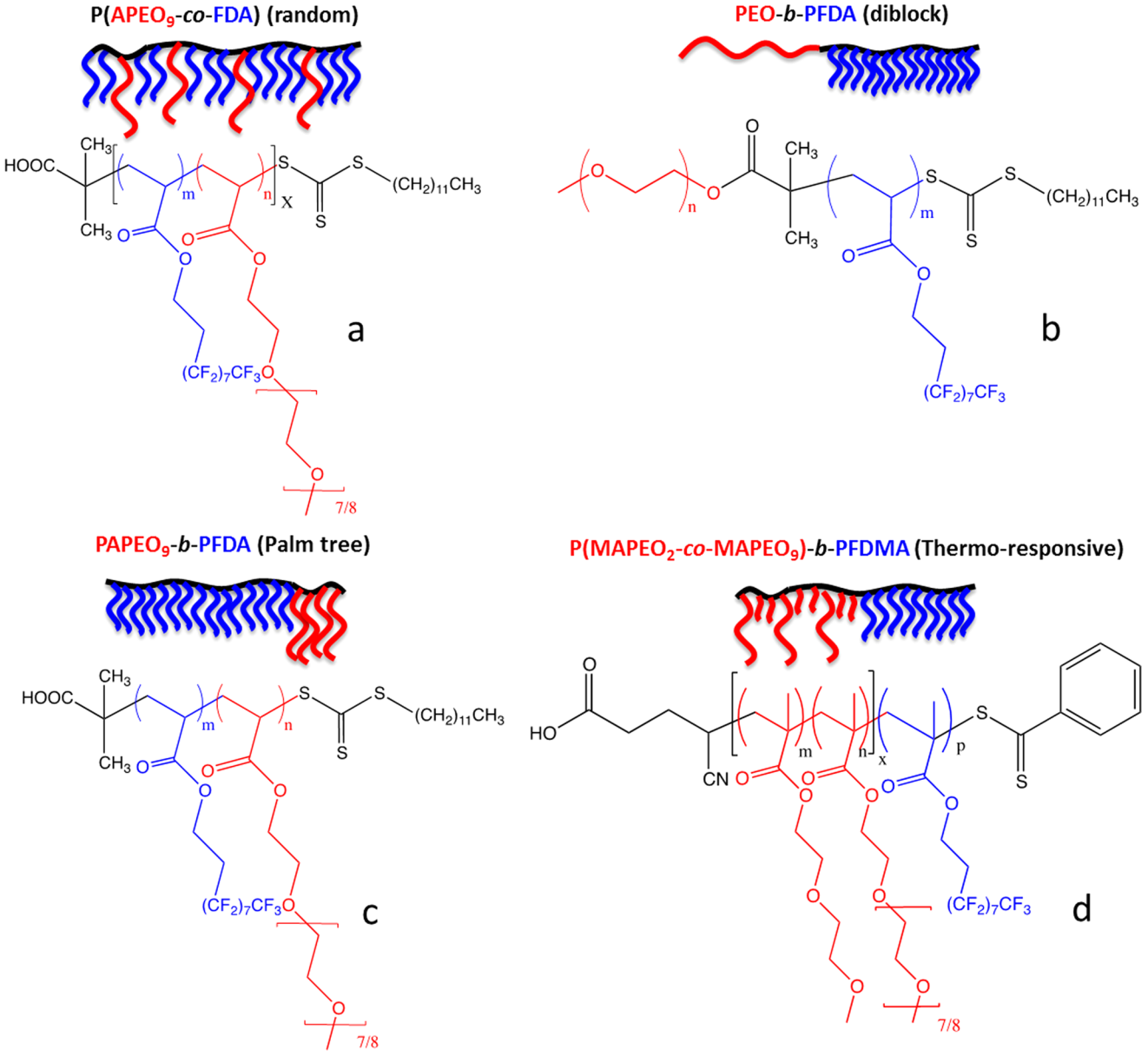

Figure 1. Molecular architecture of the P(APEO-*co*-FDA) random copolymer (a), the PEO-*b*-PFDA block copolymer (b), PFDA-*b*-PAPEO palm-tree copolymer (c), and P($(MAPEO_9)_6$-*co*-$(MAPEO_2)_{44}$)-*b*-$PFDMA_{26}$ thermoresponsive copolymer (d), synthesized by controlled radical polymerization (RAFT).

SAXS was occasionally used to study nonfluorinated molecules in CO_2 such as Dynol-604[27,28] or pluronics,[31] the technique is particularly suited for fluorinated molecules because the fluorinated compounds provide strong scattering (electron density) contrast with the $scCO_2$. Notable examples of SAXS studies on fluorinated molecules in $scCO_2$ include the formation of micelles by polystyrene-*block*-poly(perfluorooctyl acrylate) (PS-*b*-PFOA)[23] or poly(1,1-dihydroperfluorooctyl acrylate-*b*-vinyl acetate) (PFOA-*b*-PVAC),[24] as well as the stabilizing properties of copolymers made of CO_2-philic fluorinated polyacrylate (PFDA) and hydrophilic poly(ethylene oxide) (PEO).[22] Similarly, Fulton et al. used SAXS to study the aggregation of a statistical copolymer (PFOA-*g*-PEO) and proved its tendency to form small aggregates in CO_2 (around 12 nm), which can stabilize small amounts of water in their core.[22] Although several copolymers architectures (block, statistical, and so on) have been used as stabilizers in these studies,[18,21,32,33] a comparative SAXS study of the impact of the architecture is still pending.

In the present work, a series of tailor-made PFDA- and PEO-based amphiphilic copolymers, which only differ by their architecture, was prepared by controlled radical polymerization (CRP). Although they are not considered as environmentally friendly materials, we focused on fluorinated polymers because of their unequaled solubility in CO_2. More specifically, the well-known radical addition−fragmentation chain transfer (RAFT) technique was used to produce block, random, and palm-tree copolymers with the same molecular weight and composition.[34] Their behavior in $scCO_2$ was studied by SAXS as well as their ability to stabilize water droplets in $scCO_2$. Playing on the PEO architecture, it is possible to adjust the lower critical solution temperature of the hydrophilic sequence. Building on that idea, a novel thermosensitive copolymer was also synthesized by RAFT from low-molar-mass PEO-methacrylate and fluorinated

DOI: 10.1021/jp5086558
J. Phys. Chem. B 2015, 119, 1706−1716

Table 1. Macromolecular Characteristics of the Different Copolymers

architecture	copolymer composition[a]	Mn (g/mol)[b]	HFR[c]
random	$P((APEO_9)_5$-co-$FDA_{46})$	26100	0.98
block	PEO_{45}-b-$PFDA_{37}$	21000	1.22
palm-tree	$P(APEO_9)_5$-b-$PFDA_{35}$	20350	1.29
thermoresponsive	$P((MAPEO_9)_6$-co-$(MAPEO_2)_{44})$-b-$PFDMA_{26}$	25000	5.46

[a]Mn of $APEO_9$ = 454 g/mol, Mn of PEO = 2000 g/mol, Mn of $MAPEO_9$ = 475 g/mol, Mn of $MAPEO_2$ = 188 g/mol, and Mn of FDA = 518 g/mol and Mn of FDMA = 534 g/mol. [b]Total molecular weight. [c]Hydrophilic/fluorinated ratio (HFR) = number of ethylene oxide (EO) units/number of FDA units in the copolymers.

methacrylate monomers. The temperature-dependent behavior of this copolymer in CO_2/water emulsions was successfully highlighted by SAXS.

2. EXPERIMENTAL METHODS

All of the copolymers in this study were synthesized by RAFT polymerization following a procedure adapted from the literature.[34−37] In order to analyze the supramolecular structures of the copolymers in $scCO_2$, they were investigated by synchrotron SAXS at the Dutch/Belgian station (BM26b) at the European Synchrotron Radiation Facility,[46] using an autoclave equipped with two single crystal diamond windows described elsewhere.[47] The data are expressed as $I(q)$, i.e., as the scattered intensity as a function of the scattering wave vector $q = 4\pi/\lambda \sin(\theta/2)$, where θ is the scattering angle. The X-ray scattering vector range was calibrated using silver behenate as a calibrant,[48,49] and the patterns were corrected for background scattering, as explained in the Supporting Information.

The synthesis and characterization of the copolymers is explained in detail in the Supporting Information. The molecular structure of the copolymers is sketched in Figure 1 and their composition is given in Table 1. The random, block, and palm-tree copolymers are all composed of hydrophilic PEO and fluorinated CO_2-philic PFDA sequences. To specifically study the effect of the molecular architecture on the emulsifying properties of the copolymers in water/CO_2 systems, the hydrophilic and the CO_2-philic sequences were designed to have similar molecular weights in all three copolymers.[34]

In order to relate the copolymer composition to their emulsifying properties, it is customary to estimate their hydrophilic/fluorinated ratio (HFR), defined as the number of ethylene oxide (EO) units on the number of FDA units in the copolymers. The values calculated from ^1H NMR experimental data (see the Supporting Information) of the three copolymers are very similar, as reported in Table 1. Any difference in the emulsifying properties of these copolymers can therefore be attributed to their different architectures.

Homopolymers of PEO with molecular weight comparable to that of the hydrophilic moieties of the random, block, and palm-tree copolymers have a lower critical solution temperature (LCST) in water around 85 °C.[38,39] Therefore, the emulsifying properties of the latter three copolymers are not expected to exhibit any significant temperature dependence in the typical temperature range of $scCO_2$ studies, from 30 to 70 °C. By contrast, the PEO-based block of the $poly((MAPEO_9)_6$-co-$(MAPEO_2)_{44})$-b-$PFDMA_{26}$ copolymer was especially designed to exhibit temperature-dependent solubility in water in that range, by combining dimers and oligomers of ethylene oxide ($MAPEO_2$ and $MAPEO_9$). Homopolymers of $MAPEO_2$ and $MAPEO_9$ exhibit a LCST in water lower than 26 °C and higher than 90 °C, respectively, so that their combination is expected to exhibit a strong temperature dependence at intermediate temperatures.[35−37] For the synthesis of the thermoresponsive copolymer d (see Figure 1), we used a fluorinated methacrylate monomer (FDMA) rather than an acrylate in order to achieve a good control of the radical chain extension from the methacrylate-type $poly((MAPEO_9)_6$-co-$(MAPEO_2)_{44})$ macroinitiator. Because the molar mass of the hydrophilic sequence must be sufficiently high in order to exhibit a sharp LCST behavior, we targeted a molecular weight of about 11000 g/mol in $poly((MAPEO_9)_6$-co-$(MAPEO_2)_{44})$. On the other hand, the solubility in CO_2 of polymers, including perfluorinated ones, decreases when the molar mass increases. Consequently, we were compelled to lower the molecular weight of the fluorinated block (14000 g/mol) compared to the three stabilizers described previously, which results in a significantly higher HFR for the thermoresponsive copolymer (Table 1).

To a first approximation, the contribution to the SAXS signal of each copolymers subgroup is proportional to the square of β, the number of extra electrons in those groups compared to an identical volume of solvent.[40−43] Assuming that any subgroup of the copolymers contributes additively to the volume,[44] it is shown in the Supporting Information that the values of β for the fluorinated blocks are more than 10 times larger than for the PEO blocks for the first three copolymers and about 80% larger for the thermoresponsive copolymer. Therefore, the contribution of the fluorinated sequence is always much larger than the rest of the copolymer, which will only contribute to a few percent of the SAXS signal.

3. RESULTS

3.1. Copolymers Behavior in CO_2. A key property of the copolymers is their solubility in pure (i.e., dry) CO_2. The cloud points were measured as described in the Supporting Information, and they are reported in Figure 2 for a concentration of 1% (w/v) (i.e., 0.01 g of copolymer versus 1 mL of CO_2). This particular concentration unit is used throughout this work because the density of CO_2 is pressure- and temperature-dependent, which makes weight percent unpractical. The cloud points correspond to the limit of the copolymer solubility in CO_2. The high-pressure region is characterized by a unique homogeneous phase. All transition points were sharply observed experimentally.

Figure 2 shows that the copolymer with the palm-tree architecture has the highest solubility in $scCO_2$, followed closely by the random architecture. The least soluble copolymer is the thermoresponsive one, and the block copolymer has an intermediate solubility. These data can be understood from a balance between the fluorinated groups, which are well-soluble in $scCO_2$, and the PEO groups, which are opposing solubilization. In that context, the poor solubility of the thermoresponsive copolymer results simply for the lower quantity of fluorinated groups in that copolymer compared to

DOI: 10.1021/jp5086558
J. Phys. Chem. B 2015, 119, 1706−1716

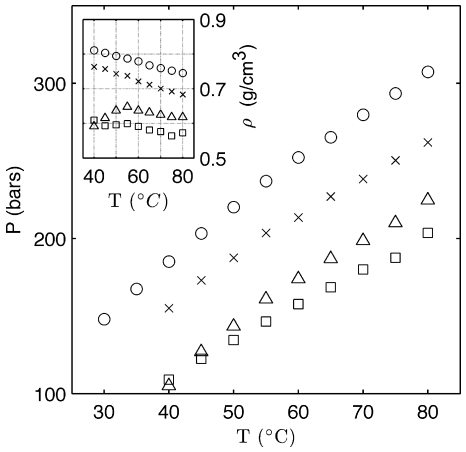

Figure 2. Cloud point curves of the different copolymers in $ScCO_2$ (at 1% (w/v) copolymer versus CO_2): random $PAPEO_9$-*co*-FDA (Δ), block PEO-*b*-PFDA (×), palm-tree $PAPEO_9$-*b*-PFDA (□), and thermoresponsive (○). The inset shows the same data plotted as the CO_2 density against temperature.

all of the others, in line with a higher HFR (see Table 1). For the other copolymers, the poorer solubility of the block copolymer compared to the palm-tree and the random architectures means that a single PEO strand is more difficult to solubilize than a series of shorter strands. The similar solubility of the palm and random architectures shows that whether the latter short strands are randomly distributed in the copolymer or are clustered at one end does not matter for the solubility.

From a physical chemistry perspective, the solubility of the copolymers has to be analyzed in terms of their free energy of mixing, which has two contributions: entropic and enthalpic. The latter contribution accounts for the energy of interaction between the copolymers and the solvent, which is expected to be proportional to the solvent density. Unlike ordinary fluids $scCO_2$ is very compressible so that the enthalpic contribution is very dependent on the pressure and temperature. In order to account for that fact, it is convenient to plot the solubility data as a function of the $scCO_2$ density rather than of the pressure. This is done in the inset of Figure 2 using a Peng−Robinson equation of state.[45] Globally, when the density of CO_2 is kept constant, the solubility of all of the copolymers considered in the present study increases with increasing temperature. This observation suggests that it is mostly the entropy of mixing of the fluorinated segments that is responsible for the temperature dependence of the solubility of the copolymers in $scCO_2$.

The SAXS patterns of the random, block, and palm-tree copolymers in $scCO_2$ are shown in Figure 3 for a variety of temperatures and pressures. In each case, the polymer concentration is 1% (w/v). The effect of a pressure increase at constant temperature was investigated first with successive dwells at P = 160, 180, and 200 bar and T = 40 °C, followed by a temperature increase to 50 °C at constant pressure P = 200 bar. At each temperature and pressure, 10 successive SAXS patterns were measured, with acquisition time of 5 min, in order to assess whether equilibrium was reached.

The SAXS patterns of the palm-tree copolymer are typical of scattering by unimers, with a plateau at low q-values, followed by a power-law decrease of the type $I \approx q^{-\alpha}$ at large q[40]. In the case of aqueous solutions, it is customary to analyze this type of data with a Debye function with α = 2, describing random polymer coils.[50,51] In the present case, however, the asymptotic exponent is significantly smaller than 2 and the following empirical function[52] was used to fit the data

$$F_{GP}(q) = \exp\left(\frac{-(qR_g)^2}{3}\right) \qquad \text{for } q \le q_1$$
$$F_{GP}(q) = \frac{D}{q^{\alpha}} \qquad \text{for } q > q_1 \tag{1}$$

where R_g is the radius of gyration of the unimers. The cutoff q_1 and the constant D are not adjustable parameters; they are related to R_g and α through $q_1 = (3\alpha/2)^{1/2}/R_g$ and $D = \exp(-(q_1R_g)^2/3)q_1^{\alpha}$. The solid lines in Figure 3 are least-squares fits of the SAXS data in the range 0.025 $Å^{-1} < q < 0.2$ $Å^{-1}$.

For most samples in Figure 3, the scattered intensity is larger than predicted by eq 1 for values of q lower than about 0.04 $Å^{-1}$, which hints at some aggregation of the unimers into larger structures. This is notably the case for the block copolymer at P = 180 bar, and particularly for random copolymer (Figure 3a). R_g of the random, block, and palm-tree copolymers all range

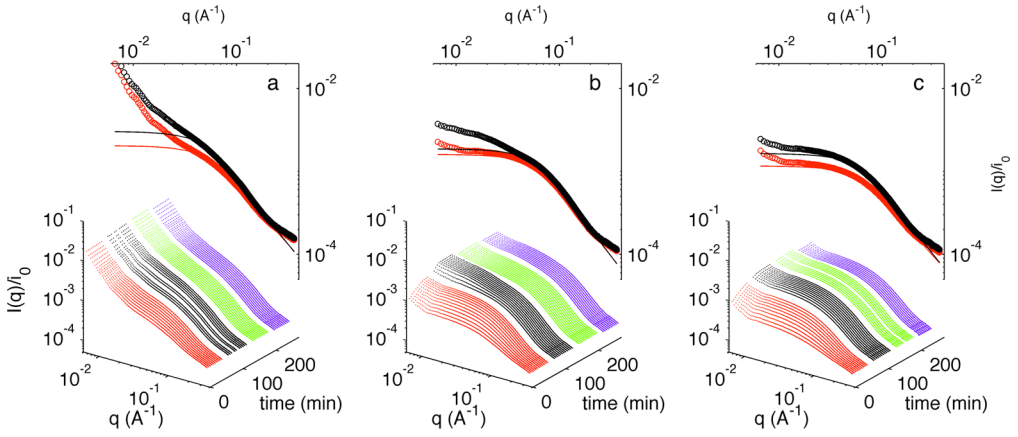

Figure 3. SAXS patterns in dry supercritical CO_2 of the copolymers with random (a), block (b), and palm-tree (c) architectures. Each color corresponds to a dwell at a given temperature and pressure, first at T = 40 °C and P = 160 bar (red), P = 180 bar (black), P = 200 bar (green), followed by a temperature increase to T = 50 °C and P = 200 bar (purple). The insets are the last patterns of the first two dwells, together with a fit with eq 2 for q > 0.025 $Å^{-1}$ (solid lines). The SAXS patterns are qualitatively similar at P = 200 bar and at T = 50 °C.

DOI: 10.1021/jp5086558
J. Phys. Chem. B 2015, 119, 1706−1716

from 18 to 22 Å, and the scattering exponents α range from 1.4 to 1.7. The latter values are very close to the theoretical value 5/3 expected for fully swollen polymer chains in a good solvent.[53,54]

The combination of the cloud point pressure data with the SAXS shows that although the palm-tree and the random copolymers are both very soluble in $scCO_2$ (Figure 2), the reason for this is different in both cases. In the case of the palm-tree and the block copolymers, the SAXS shows that only unimers are present in the solution, which points at small isolated PEO globules solubilized by a single protruding CO_2-philic sequence. This is in striking contrast with the copolymer with random architecture, the SAXS of which points to the existence of an extended supramolecular assembly in which a large number of copolymers are assembled, possibly via shared collapsed CO_2-phobic sequences. The overall decrease of the SAXS intensity in Figure 3a extends over the entire q range, which shows that the size of these copolymer assemblies is larger than the lower resolution limit of the SAXS, about 60 nm.

3.2. Copolymer Behavior in Water/CO_2 Mixtures. The major objective of the present work is to understand the impact of the copolymer architecture on their emulsifying properties in $scCO_2$, which entails studying their behavior in water/CO_2 mixtures. This was first investigated macroscopically using the method described in the Supporting Information: the copolymers were used to try stabilizing an aqueous solution of amaranth in $scCO_2$, and the presence of stable water droplets was assessed visually by the red hue of the mixture.

Figure 4 shows the emulsions obtained at 40 °C with the random, block, and palm-tree copolymers (columns) for different pressures ranging from 180 to 300 bar (rows), 1 h after stopping the homogenizing and stirring. The color of the solutions containing the random and block copolymers evidences the presence of stable amaranth-containing water droplets, efficiently stabilized by the used copolymer. By contrast, the transparency of the solution with the palm-tree copolymer means that the latter macromolecule is unable to stabilize the emulsion. In the case of the experiments done at 300 bar (Figure 4, bottom row), the trend is even clearer: the opacity of the solution with the block copolymer is due to an extremely high concentration of amaranth-containing water in the $scCO_2$. The experiments were also done at 200 bar (not shown), and the results where visually indistinguishable from those at 180 bar.

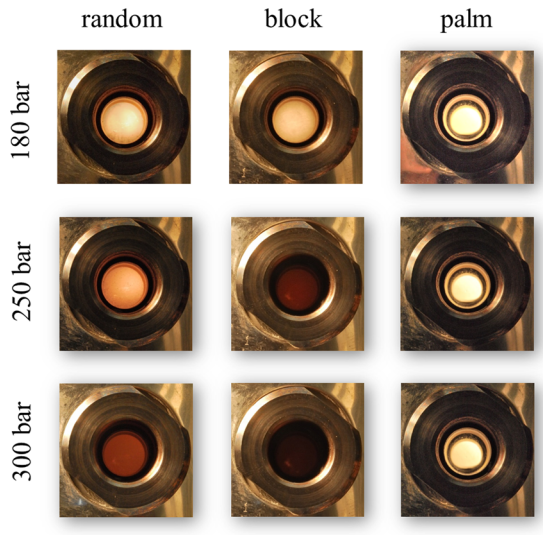

Figure 4. Water/CO_2 emulsification experiments carried out at 40 °C in a high-pressure view cell with different copolymer stabilizers. The color testifies to the presence of amaranth-containing stable water droplets in CO_2. From left to right, random, block and palm-tree architectures, and from top to bottom, 180, 250, and 300 bar. In all cases, the amount of stabilizer is 1% (w/v) vs CO_2 and the amount of water is 4% (w/v) vs CO_2. The pictures were taken 1 h after stopping the stirring and homogenization. In the case of the block copolymer at 300 bar, the opacity of the mixture points to the excellent stability of the emulsion.

The different emulsifying properties of the copolymers are also confirmed by the time evolution of the emulsions once the stirring is stopped. During homogenization and stirring, all emulsions are reddish and opaque. Once the stirring is stopped, the solution with the palm-tree copolymer becomes transparent in a matter of minutes. The solution with the block copolymer at 300 bar remains opaque for more than 24 h emphasizing the excellent stabilizing capacity of this architecture.

In order to understand at the nanometer scale the strikingly different emulsifying properties of the three copolymers, despite their comparable HFR and molecular weight, the water/CO_2 emulsions were analyzed by SAXS. Figure 5 shows the SAXS data of the copolymers in CO_2 with 1 and 4% (w/v) water relative to the total volume of the setup.

The SAXS pattern of the emulsion with the random copolymer shows that the large-scale supramolecular structure detected in the dry CO_2 disappears when water is present; the SAXS of the emulsion is identical to the SAXS of the isolated fluorinated strands (which we have referred to previously as the unimers). Nevertheless, a stable CO_2/water emulsion was observed with the random stabilizer (Figure 4, left column). This means that the structures formed in the presence of water are much larger than the lower resolution limit of the SAXS (about 60 nm) so that they do not scatter in the observed angular range. In other words, the difference between the SAXS patterns with and without water hints at the presence of water droplets larger than about 60 nm.

In the case of the block copolymer, the SAXS patterns show that structures are formed in the presence of water, which were absent in dry CO_2 (Figure 5b). The patterns are typical of spherical micelle structures, with a two-step decrease of the intensity when increasing q: the first decrease corresponds to the overall micelle and the second to the inner structure of the lyophilic moieties of the polymer.[55]

Finally, in the case of the palm-tree copolymer, only the scattering by the fluorinated sequences is observed in the SAXS. Based on this sole observation we cannot *a priori* rule out the possibility of droplets much larger than the lower resolution limit of the SAXS, similar to the situation of the random copolymer. However, the presence of large micelle structures in CO_2 is unlikely based on the macroscopic observations of Figure 4, which points at the absence of any dispersed water in the solution.

In order to quantitatively analyze the SAXS data of the block copolymer stabilized emulsion, we considered the micelle model sketched in Figure 6. It consists of a spherical water-rich core of radius R in which the hydrophilic PEO blocks of the copolymer are dissolved, surrounded by a corona containing fluorinated blocks. The configuration of the latter is characterized by a radius of gyration R_g. Calculating the form factor of such an object would require considering the self-

DOI: 10.1021/jp5086558
J. Phys. Chem. B 2015, 119, 1706−1716

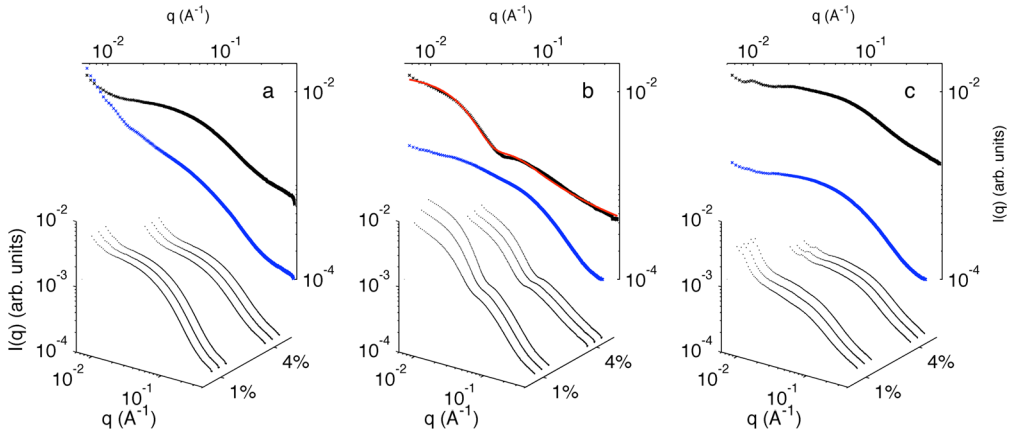

Figure 5. Small-angle scattering patterns of water/CO_2 emulsions stabilized with the copolymers having random (a), block (b), and palm-tree (c) architectures. The temperature is 40 °C, and the pressure is 180 bar. Two series of data are plotted with 1 and 4% (w/v) water. The three patterns for each water concentration were measured at intervals of 10 min to ascertain that equilibrium was reached. In the background, the last pattern measured with 4% (w/v) water is compared with the corresponding copolymer in dry CO_2 (blue). In the case of the block copolymer, the red curve is the least-squares fit of the data with the emulsion model shown in Figure 6.

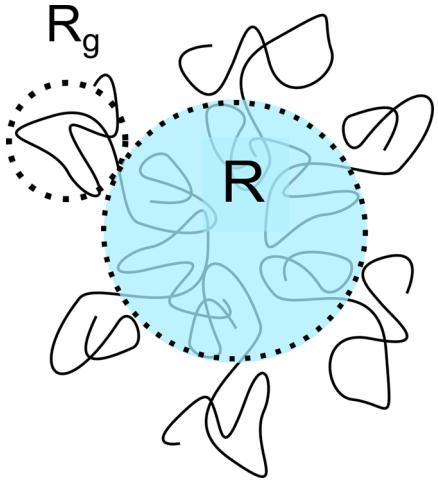

Figure 6. Sketch of the stabilized nanodroplet model used to analyze the SAXS data: R_g is the radius of gyration of the fluorinated lyophilic moieties, which contain most of the electrons, and R is the radius of the water-rich spherical core.

correlations and all possible cross-correlations between the three phases—namely, the fluorinated blocks, the PEO blocks, and water—which would amount to a total of six terms. However, as we discussed earlier, most of the excess electrons in the polymer are in the fluorinated blocks (see Supporting Information Table S2), which contribute the most to the SAXS. Moreover, the electron density of the PEO is 0.37 $e^-/Å^3$ (Supporting Information Table S1), which is very close to that of water (0.33 $e^-/Å^3$). Therefore, it is reasonable to approximate the form factor of the stabilized droplet by neglecting the contribution of the inner structure of the water-rich core. In this case, the form factor reduces to the well-known expression calculated by Pedersen and Gerstenberg for block copolymer micelles[55]

The form factor of block copolymer micelles is written as follows

$$F_{mu}(q) = \beta_s^2 F_s(q) + N_{agg}\beta_c^2 F_c(q) + N_{agg}(N_{agg} - 1)\beta_c^2 S_{cc}(q) + 2N_{agg}\beta_c\beta_s S_{cs}(q) \quad (2)$$

where β_s is the total excess electrons in the spherical core, which contains here both the lyophobic (i.e., hydrophilic) moieties of all of the copolymers forming the emulsion as well as water, β_c is the total excess electrons in the lyophilic (i.e., fluorinated) moiety of a single copolymer, and N_{agg} is the aggregation number, corresponding to the number of copolymers in a single emulsion nanodroplet. The q-dependent functions in eq 2 are the same as in the original work.[55] They are the form factor of the spherical core $F_s(q)$ and of the individual chains in the corona $F_c(q)$ and the cross-correlations between the chains $S_{cc}(q)$ and between the chains and the spherical core $S_{cs}(q)$.

In eq 2, the total excess of electrons in the spherical core of the emulsion is calculated by adding the contributions of water and of the PEO blocks of all the aggregated copolymers. This results in

$$\beta_s = \frac{4}{3}\pi R^3(\rho_{H_2O} - \rho_{CO_2}) + N_{agg}V_{PEO}(\rho_{PEO} - \rho_{H_2O}) \quad (3)$$

where ρ_{H_2O}, ρ_{CO_2}, and ρ_{PEO} are the electron densities of the water, CO_2, and PEO blocks of the copolymers and V_{PEO} is the total volume of the PEO block, as calculated in the Supporting Information Table S2. Another modification compared to ref 55 concerns the assumed configuration of the lyophilic polymer blocks in the corona. In the original form factor, the polymer configuration in the lyophilic corona of the micelle is assumed to obey Gaussian statistics, which leads to a Debye form factor for $F_c(q)$. Because the configuration of the lyophilic moiety is expected to be very similar in the unimers and in the corona of the micelle-like structure, it is natural to use the same form factor in both cases. This is particularly true in the present context because it is mostly the fluorinated CO_2-philic moiety that contributes to the SAXS signal. Therefore, we model $F_c(q)$ using the same empirical expression as in eq 1. The cross-correlation $S_{sc}(q)$ is calculated from the scattered amplitude $\psi(q)$ of the chains in the corona, assuming $\psi(q) = \sqrt{F_c}$, which is equivalent to making a mean-field approximation. We also made the customary assumption that the centers of the polymer coils in the corona are at a distance $R_g/2$ from the surface of the spherical core.

DOI: 10.1021/jp5086558
J. Phys. Chem. B 2015, 119, 1706−1716

The SAXS intensity of the block copolymer with 4% (w/v) water (Figure 5b) was fitted to the microemulsion model under the form

$$I(q) = A_{mu}F_{mu}(q; R, N_{agg}) + A_{u}F_{GP}(q) + Bq^{-b} \quad (4)$$

The first term, with prefactor A_{mu}, describes the scattering of the microemulsion; the second term, proportional to A_u, accounts for the possible presence of unimers in the solution; and the last term represents the background scattering, which we model as a power law. The latter background scattering is clearly visible in Figures 3 and 5 as the linear region in the graphs above $q \sim 0.2$ Å^{-1}; for the fitting, the exponent is fixed once and for all at $b = 0.4$. Similarly, we assumed that the configuration of the chains in the corona were identical to the one in the unimers, and we fixed the values $R_g = 20$ Å and $\alpha = 5/3$. The only two adjustable parameters for the fit—besides the prefactors A_{mu}, A_u, and B—are therefore the radius of the water-rich core and the aggregation number. The least-squares fit leads to a radius $R = 95$ Å for the water core of the micelle and an aggregation number $N_{agg} = 55$; the fitted function is shown as a red line in Figure 5b.

The aggregation number can be expressed in a more intuitive way in terms of the average area a occupied by a copolymer at the surface of the nanodroplet of radius R, namely, $a = 4\pi R^2/N_{agg}$. The values obtained from the fit correspond to $a = 21$ nm^2. Another way of expressing the aggregation number is via the water to polymer mass ratio. Using the values in Supporting Information Table S2 for the total volume of the PEO blocks, one finds that the nanodroplets observed in the SAXS contain approximately two times more water than polymer. This ratio has to be compared with the macroscopic composition of the emulsion according to which the total masses of water and polymer in the emulsion are identical.

The SAXS of the emulsion with 1% (w/v) water was also fitted with the emulsion model (not shown). The time evolution observed in Figure 5 can be entirely attributed to an increase of the prefactor A_{mu}, i.e., to a concentration effect, while the core radius and the surface coverage remained approximately constant with time, with values $R = 95$ Å and $a = 142$ nm^2. These values correspond to an aggregation number as little as 8 and water-to-polymer mass ratio as large as 13.

Finally, the properties of the poly((MAPEO$_9$)$_6$-*co*-(MAPEO$_2$)$_{44}$)-*b*-PFDMA$_{26}$ copolymer (structure 4 in Figure 1) were investigated in order to assess the possibility of designing thermoresponsive water/scCO$_2$ emulsions and to observe the effect of CO$_2$ on the transition temperatures. The LCST of the thermoresponsive PEO-containing sequence alone was found by turbidimetry to be 41.3 °C in pure water (see the Supporting Information). Combining the PEO-containing sequence with the strongly hydrophobic blocks of fluorinated methacrylate may result in a change of its LCST, which cannot be studied directly because the fluorinated copolymer is not soluble in pure water. Moreover, water acidification by CO$_2$ may also modify the LCST of the PEO-containing sequence of the copolymer. Optical measurements show that stable water/CO$_2$ emulsions are obtained at 200 bar and 35 °C with the poly((MAPEO$_9$)$_6$-*co*-(MAPEO$_2$)$_{44}$)-*b*-PFDMA$_{26}$ (Supporting Information Figure S2). When increasing the temperature to 55 °C, i.e., above the LCST of the PEO sequence alone in pure water, destabilization of the emulsion was expected. However, only a slight color change was detected from dark to light orange. In order to gain more insight into the thermoresponsiveness of the poly((MAPEO$_9$)$_6$-*co*-(MAPEO$_2$)$_{44}$)-*b*-PFDMA$_{26}$ copolymer under water/CO$_2$ emulsion, SAXS measurements were performed on such emulsions at various temperatures.

The SAXS patterns in scCO$_2$ with 4% (w/v) water and 1% (w/v) poly((MAPEO$_9$)$_6$-*co*-(MAPEO$_2$)$_{44}$)-*b*-PFDMA$_{26}$ at 200 bar are shown in Figure 7 for temperatures ranging from 34 to

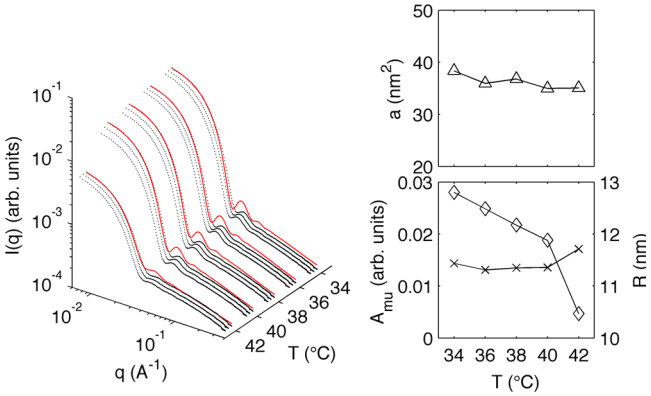

Figure 7. SAXS patterns measured on the thermoresponsive copolymer (left) at $P = 200$ bar and temperatures ranging from 34 to 42 °C. The various patterns shown for a single temperature are measured every 5 min to check the equilibration time; the red lines are least-squares fits with the nanodroplet model of Figure 6. The values of the prefactor A_{mu} (◊), of the radius R (×) of the water-rich core, and of the area occupied by a copolymer at the water/CO$_2$ interface (Δ) are plotted on the right.

42 °C, i.e., encompassing the LCST of the hydrophilic sequence of 41.3 °C. These data were measured in the order of decreasing temperatures, starting from 42 °C. At each temperature decrease, the CO$_2$ pressure was first adjusted by adding CO$_2$ to the reactor, followed by 5 min homogenization. The homogenizer was then stopped, and three successive SAXS patterns were measured with time intervals of 5 min, in order to ascertain that equilibrium was reached.

The SAXS patterns of the emulsion stabilized with the thermoresponsive copolymer are qualitatively similar to those of the block copolymer, i.e., of spherical micelle-like structures. Interestingly, they are strongly temperature-dependent; the scattered intensity increases by approximately a factor of 3 when decreasing the temperature from 42 to 34 °C (note the logarithmic scales in Figure 7). This observation suggests that the temperature transition of the PEO-containing segment of the poly((MAPEO$_9$)$_6$-*co*-(MAPEO$_2$)$_{44}$)-*b*-PFDMA$_{26}$ in water/CO$_2$ emulsion is close to the LCST of the poly((MAPEO$_9$)$_6$-*co*-(MAPEO$_2$)$_{44}$) block alone in pure water (41.3 °C). It has also to be kept in mind that the density of scCO$_2$ at $P = 200$ bar increases from 0.24 to 0.26 e/Å^3 when the temperature is decreased from 42 to 34 °C. This means that the significant temperature dependence of the SAXS in Figure 7 underestimates the actual changes in the nanostructure of the emulsion.

In order to take full account of the changes in CO$_2$ density, the SAXS data of the emulsion were also fitted with the nanodroplet model. For the fit, the excess number of electrons in the fluorinated and hydrophilic sequences were determined from the data of Supporting Information Table S2, and the actual CO$_2$ density was used in eq 3. Because the fluorinated sequence is significantly smaller in the thermoresponsive

DOI: 10.1021/jp5086558
J. Phys. Chem. B 2015, 119, 1706−1716

copolymer compared to the random, block, and plam-tree copolymers (Supporting Information Table S2), a smaller value of R_g had to be used for the fit. When R_g is treated as an adjustable parameter for the least-squares fit, it is found to be randomly scattered from values between 5 and 15 Å. We therefore arbitrarily imposed the value R_g = 10 Å, but the conclusions are left unchanged if a slightly different value is used. The best fit of the data is shown in red in Figure 7, together with the temperature dependence of the fitted parameters A_{mu}, R, and a.

Globally, the nanodroplet model can be used to describe the SAXS data. There are some weak oscillations in the curves of the model that are absent in the data, which hints at a slight dispersity of the nanodroplets. The nanodroplets are slightly larger with the thermoresponsive copolymer than with the block copolymer (R = 11 nm compared to 10 nm), and the aggregation number is of the order of 45. These values convert to an area about a = 37 nm and to a water-to-polymer mass ratio close to 3.

Concerning the temperature dependence the largest effect is on the prefactor A_{mu}, which is approximately proportional to the number concentration. Comparatively, the effect of temperature on the radius R of the nanodroplet and on the area occupied by a copolymer at the water/CO_2 interface is minimal. It is striking that the number of nanodroplets decreases sharply raising the temperatures from 40 to 42 °C, which interval straddles the critical temperature of the hydrophilic segment (41.3 °C) measured independently in pure water.

4. DISCUSSION

The architecture of the copolymers was found to have an effect on the solubility of the copolymers in CO_2, as evidenced by the different cloud point pressures of the copolymers (Figure 2). Quite generally, a central property of amphiphilic molecules in solution is their ability to form supramolecular assemblies, which contributes to minimizing the direct contact of the lyophobic sequences with the solvent. From that point of view, the similarly low cloud point pressures of the random and palm-tree copolymers would hint at similar supramolecular assemblies. Interestingly, the SAXS patterns of these two copolymers in CO_2 are distinctly different. The SAXS of the random copolymer clearly evidence the formation of large and disordered supramolecular structures, with an overall power-law scattering with exponent close to −2 (Figure 3a). By contrast, in the case of the palm-tree and the block copolymer, the SAXS shows that only unimers, i.e., isolated macromolecules, are present.

The ability of the three copolymers to stabilize water/CO_2 emulsions was investigated both at the nanometer scale by SAXS (Figure 5) and at the macroscopic scale by using amaranth as a visual marker for the presence of dispersed water droplets (Figure 4). Here again, the three copolymers exhibit very different properties, which can only be attributed to their different architectures. The random copolymer is effective at stabilizing water/CO_2 emulsions. The loose supramolecular structure previously detected for the random copolymer in CO_2 is no longer observed in the presence of water. In the latter situation, the copolymer is likely to be positioned at the water/CO_2 interface, with water droplets larger than the lower resolution limit of the SAXS. Surprisingly, based on the macroscopic observation in the presence of amaranth, the palm-tree copolymer is seen to be unable to stabilize water/CO_2 emulsions at all. Whatever large supramolecular structures these copolymers made in CO_2, which we hypothesized when discussing the SAXS of Figure 3c, these structures either cannot form in the presence of water or they cannot remain in solution. The most stable emulsions were obtained with the copolymer having the block architecture, i.e., the copolymer that is the less soluble in CO_2. SAXS revealed that the latter emulsions consisted of spherical droplets around 20 nm in diameter, similar to Figure 6, with a water-to-polymer mass ratio close to 2.

It is quite interesting to compare the emulsifying properties of the three copolymers with earlier results concerning their effect on the water/trifluorotoluene (TFT) interfacial tension.[34] The water/TFT interface can be used as a model for the water/CO_2 interface because water and TFT are not miscible and the fluorinated sequences of the copolymers are soluble in TFT. These earlier works based on the pendant drop method showed that the most tensioactive of the three copolymers was the one with block architecture, followed by the palm-tree, and the one with random architecture was the least tensioactive. The good tensioactive properties of the palm-tree copolymer may first seem to be at odds with its inability to stabilize water/CO_2 emulsions. To explain this, it has to be noted that the curvature of the interface is very different in both experimental situations. The typical radius of curvature is about a millimeter when measuring a surface tension by the pendant drop method, and a few nanometers in the case of an emulsion. The very large curvature involved in the latter case makes steric effects likely (see Figure 8). The palm-tree architecture, having a large number of PEO branches very close to the water/CO_2 interface, is extremely unfavorable to the formation of objects with a large curvature.

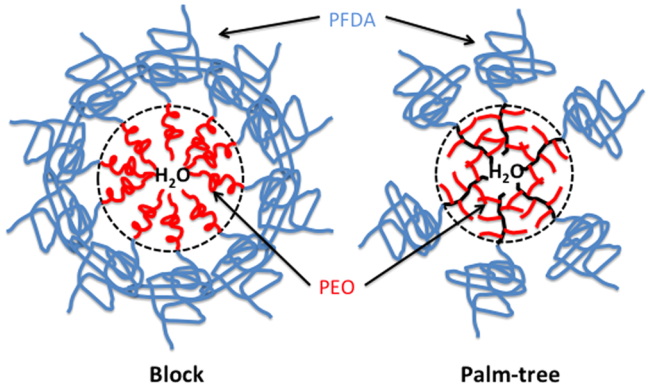

Figure 8. Sketch of the architecture-dependent steric hindrance effects for the stabilization of nanometer-sized water droplets. The branched palm-tree architecture is less favorable to the stabilization of curved interfaces than the linear block architecture.

From a steric hindrance point of view, the hydrophilic sequence of the poly((MAPEO$_9$)$_6$-*co*-(MAPEO$_2$)$_{44}$)-*b*-PFDMA$_{26}$ is expected to be intermediate between the block and the palm-tree copolymers. Indeed, the nanodroplets stabilized by the thermoresponsive copolymer are slightly larger compared to those formed in the presence of the block copolymer. Finally, we also further demonstrated the thermoresponsiveness of the latter copolymer, which stabilizes more water droplets in scCO_2 below the LCST of its hydrophilic sequence. This observation offers the prospect of engineering thermoresponsive scCO_2 /water emulsions.

DOI: 10.1021/jp5086558
J. Phys. Chem. B 2015, 119, 1706−1716

5. CONCLUSION

We have used small-angle scattering to analyze at the nanometer scale the properties and supramolecular structures of a series of amphiphilic fluorinated copolymers in supercritical CO_2, as well as in water/CO_2 emulsions. Reversible addition−fragmentation chain transfer polymerization (RAFT) enabled us to synthesize copolymers with comparable molecular weight and composition, but with distinctly different molecular architectures. We investigated a random, a block, and palm-tree copolymers.

Small-angle scattering shows that the block and palm-tree copolymers are mainly present as unimers in CO_2 and that they accordingly do not assemble at the supramolecular level. By contrast, the random copolymer was seen to form large disordered aggregates.

The molecular architecture was also found to have an impact on the ability of the copolymers to stabilize water emulsions in CO_2. This was first assessed macroscopically, using amaranth as a visual marker for the presence of water. This procedure showed that the most effective architecture is by far the block, followed by the random. The palm-tree architecture is not able to stabilize any emulsion, even at pressures as high as 300 bar. SAXS shows that the emulsions consist of water droplets about 20 nm across in the case of the block architecture and of droplets larger than the resolution of the SAXS (about 100 nm) for the random architecture. Expectedly, only unimers in CO_2 are detected by SAXS in the case of the copolymer with palm-tree architecture.

In addition to these three main architectures, a fourth thermoresponsive copolymer was also synthesized by RAFT. Below the LCST of the hydrophilic sequence, that copolymer was found to stabilize nanometer-sized droplets. When the LCST is approached and eventually crossed, the size of the droplets remains constant but their number decreases significantly.

Overall, this study provides overwhelming evidence for the impact of the architecture of amphiphilic fluorinated copolymers on their behavior and supramolecular assembly in dry supercritical CO_2, as well as in water/CO_2 emulsions. It also rationalizes their water-in-CO_2 emulsifying power and paves the way for the rational design of even more suitable and stimuli-responsive stabilizers for the supercritical CO_2 technology.

■ ASSOCIATED CONTENT

Supporting Information

Text describing experimental details concerning the synthesis and characterization of the copolymers, the determination of the cloud points, the *in situ* SAXS measurements in supercritical CO_2, the estimation of the electron density of the subgroups of the copolymers relevant to the SAXS data analysis, and accompanying references, tables listing monomer and water properties and calculation of their electron densities and properties of molecular blocks and calculation of their total excess electrons, and figures showing the experimental setup and water/CO_2 emulisification optical cloud point experiments. This material is available free of charge via the Internet at http://pubs.acs.org.

■ AUTHOR INFORMATION

Corresponding Authors

*(A.D.) E-mail: adebuigne@ulg.ac.be. Tel.: +32 4 366 3565.

*(C.J.G.) E-mail: cedric.gommes@ulg.ac.be. Tel.: +32 4 366 3545.

Notes

The authors declare no competing financial interest.

■ ACKNOWLEDGMENTS

A.D. and C.J.G. both have Research Associate positions with the F.R.S.-FNRS (Belgium). We are grateful to the Fonds Wetenschappelijk Onderzoek (Vlaanderen) and the Nederlandse Organisatie voor Wetenschappelijk Onderzoek (NWO) for supporting the DUBBLE project at the ESRF. C.J.G. is also grateful to Prof. Bart Goderis (KULeuven) for fruitful discussions. D.H.M. thanks the Dutch Polymer Institute (DPI) for funding. D.A. and A.D. thank the "Belgian Science Policy" for financial support in the frame of the Interuniversity Attraction Poles Programme (P7/05)−Functional Supramolecular Systems (FS2). D.A. is also grateful to the "Fonds de la Recherche pour l'Industrie et l'Agriculture" (FRIA) and to "Région Wallonne" and the FEDER in the frame of the POLYTISS project for their financial support.

■ REFERENCES

(1) Gever, S.; Schulmeyr, J. Ecological and gentle technology—CO_2 Extraction and Its Use in Food Technology. *Innovations Food Technol.* **2007**, *34*, 44−46.

(2) Diaz-Reinoso, B.; Moure, A.; Dominguez, H.; Parajo, J. C. Supercritical CO_2 Extraction and Purification of Compounds with Antioxidant Activity. *J. Agric. Food Chem.* **2006**, *54* (7), 2441−69.

(3) Mikami, K. *Green Reaction Media in Organic Synthesis*; Wiley-Blackwell, 2005; pp 125−182.

(4) DeSimone, J. M.; Tumas, W. *Green Chemistry Using Liquid and Supercritical Carbon Dioxide*, Oxford University Press: Oxford, U.K., 2003; 48−63

(5) Park, E. J.; Richez, A. P.; Birkin, N. A.; Lee, H.; Arrowsmith, N.; Thurecht, K. J.; Howdle, S. M. New Vinyl Ester Copolymers as Stabilizers for Dispersion Polymerization in $scCO_2$. *Polymer* **2011**, *52* (24), 5403−5409.

(6) Galia, A.; Giaconia, A.; Iaia, V.; Filardo, G. Synthesis of Hydrophilic Polymers in Supercritical Carbon Dioxide in the Presence of a Siloxane-Based Macromonomer Surfactant: Heterogeneous Polymerization of 1-Vinyl-2 Pyrrolidone. *J. Polym. Sci., Part A: Polym. Chem.* **2003**, *42* (1), 173−185.

(7) Ma, Z.; Lacroix-Desmazes, P. Dispersion Polymerization of 2-Hydroxyethyl Methacrylate Stabilized by a Hydrophilic/CO_2-Philic Poly(ethylene oxide)-b-poly(1,1,2,2-tetrahydroperfluorodecyl acrylate) (PEO-b-PFDA) Diblock Copolymer in Supercritical Carbon Dioxide. *Polymer* **2004**, *45* (20), 6789−6797.

(8) Shiho, H.; Desimone, J. M. Dispersion Polymerization of Styrene in Supercritical Carbon Dioxide Utilizing Random Copolymers Containing a Fluorinated Acrylate for Preparing Micron-Size Polystyrene Particles. *J. Polym. Sci., Part A: Polym. Chem.* **2000**, *38* (7), 1146−1153.

(9) Hsiao, Y.-L.; Maury, E. E.; DeSimone, J. M.; Mawson, S.; Johnston, K. P. Dispersion Polymerization of Methyl Methacrylate Stabilized with Poly(1,1-dihydroperfluorooctyl acrylate) in Supercritical Carbon Dioxide. *Macromolecules* **1995**, *28* (24), 8159−66.

(10) Carson, T.; Lizotte, J.; Desimone, J. M. Dispersion Polymerization of 1-Vinyl-2-pyrrolidone in Supercritical Carbon Dioxide. *Macromolecules* **2000**, *33* (6), 1917−1920.

(11) Shiho, H.; DeSimone, J. M. Dispersion Polymerization of 2-Hydroxyethyl Methacrylate in Supercritical Carbon Dioxide. *J. Polym. Sci., Part A: Polym. Chem.* **2000**, *38* (20), 3783−3790.

(12) Psathas, P. A.; Janowiak, M. L.; Garcia-Rubio, L. H.; Johnston, K. P. Formation of Carbon Dioxide in Water Miniemulsions Using the Phase Inversion Temperature Method. *Langmuir* **2002**, *18* (8), 3039−3046.

DOI: 10.1021/jp5086558
J. Phys. Chem. B 2015, 119, 1706−1716

(13) Lee, C. T., Jr.; Psathas, P. A.; Johnston, K. P.; DeGrazia, J.; Randolph, T. W. Water-in-Carbon Dioxide Emulsions: Formation and Stability. *Langmuir* **1999**, *15* (20), 6781−6791.
(14) Yazdi, A. V.; Beckman, E. J. Design of highly CO_2-soluble chelating agents for carbon dioxide extraction of heavy metals. *J. Mater Res.* **1995**, *10* (3), 530−537.
(15) Yazdi, A. V.; Lepilleur, C.; Singley, E. J.; Liu, W.; Adamsky, F. A.; Enick, R. M.; Beckman, E. J. Highly Carbon Dioxide Soluble Surfactants, Dispersants and Chelating Agents. *Fluid Phase Equilib.* **1996**, *117* (1−2), 297−303.
(16) Shiho, H.; DeSimone, J. M. Dispersion Polymerization of Glycidyl Methacrylate in Supercritical Carbon Dioxide. *Macromolecules* **2001**, *34* (5), 1198−1203.
(17) Giles, M. R.; Griffiths, R. M. T.; Aguiar-Ricardo, A.; Silva, M. M. C. G.; Howdle, S. M. Fluorinated Graft Stabilizers for Polymerization in Supercritical Carbon Dioxide: The Effect of Stabilizer Architecture. *Macromolecules* **2000**, *34* (1), 20−25.
(18) Dickson, J. L.; Psathas, P. A.; Salinas, B.; Ortiz-Estrada, C.; Luna-Barcenas, G.; Hwang, H. S.; Lim, K. T.; Johnston, K. P. Formation and Growth of Water-in-CO_2 miniemulsions. *Langmuir* **2003**, *19* (12), 4895−4904.
(19) Lepilleur, C.; Beckman, E. J. Dispersion Polymerization of Methyl Methacrylate in Supercritical CO_2. *Macromolecules* **1997**, *30* (4), 745−756.
(20) Baran, N.; Deniz, S.; Akguen, M.; Uzun, I. N.; Dincer, S. Dispersion Polymerization of Styrene in Supercritical Carbon Dioxide using Monofunctional Perfluoropolyether and Silicone-Containing Fluoroacrylate Stabilizers. *Eur. Polym. J.* **2005**, *41* (5), 1159−1167.
(21) Shiho, H.; DeSimone, J. M. Dispersion Polymerization of Acrylonitrile in Supercritical Carbon Dioxide. *Macromolecules* **2000**, *33* (5), 1565−1569.
(22) Fulton, J. L.; Pfund, D. M.; McClain, J. B.; Romack, T. J.; Maury, E. E.; Combes, J. R.; Samulski, E. T.; DeSimone, J. M.; Capel, M. Aggregation of Amphiphilic Molecules in Supercritical Carbon Dioxide: A Small Angle X-ray Scattering Study. *Langmuir* **1995**, *11* (11), 4241−9.
(23) Londono, J. D.; Dharmapurikar, R.; Cocharn, H. D.; Wignall, G. D.; McClain, J. B.; Betts, D. E.; Canelas, D. A.; DeSimone, J. M.; Samulski, E. T.; Chillura-Martino, D.; et al. The Morphology of Block Copolymer Micelles in Supercritical Carbon Dioxide by Small-Angle Neutron and X-ray Scattering. *J. Appl. Crystallogr.* **1997**, *30* (5), 690−695.
(24) Liu, L.-Z.; Cheng, Z.; Inomata, K.; Zhou, S.; Chu, B. Synchrotron SAXS and Laser Light Scattering Studies of Aggregation Behavior of Poly(1,1-dihydroperfluorooctyl acrylate-*b*-vinyl acetate) Diblock Copolymer in Supercritical Carbon Dioxide. *Macromolecules* **1999**, *32* (18), 5836−5845.
(25) Lo Celso, F.; Triolo, A.; Triolo, F.; Donato, D. I.; Steinhart, M.; Kriechbaum, M.; Amenitsch, H.; Triolo, R. Synchrotron SAXS Investigation on Aggregation Phenomena in Supercritical CO_2. *Eur. Phys. J. E: Soft Matter Biol. Phys.* **2002**, *8* (3), 311−314.
(26) Triolo, A.; Lo Celso, F.; Triolo, F.; Amenitsch, H.; Steinhart, M.; Thiyagarajan, P.; Wells, S.; DeSimone, J. M.; Triolo, R. Kinetics of Block Copolymer Aggregation in Supercritical CO_2. *J. Non-Cryst. Solids* **2002**, *307−310*, 725−730.
(27) Liu, J.; Han, B.; Li, G.; Zhang, X.; He, J.; Liu, Z. Investigation of Nonionic Surfactant Dynol-604 Based Reverse Microemulsions Formed in Supercritical Carbon Dioxide. *Langmuir* **2001**, *17* (26), 8040−8043.
(28) Liu, J.; Zhang, J.; Mu, T.; Han, B.; Li, G.; Wang, J.; Dong, B. An Investigation of Non-fluorous Surfactant Dynol-604 Based Water-in-CO_2 Reverse Micelles by Small Angle X-ray Scattering. *J. Supercrit. Fluids* **2003**, *26* (3), 275−280.
(29) Zhang, J.; Han, B.; Liu, J.; Zhang, X.; Yang, G.; He, J.; Liu, Z.; Jiang, T.; Wang, J.; Dong, B. Effect of Compressed CO_2 on the Size and Stability of Reverse Micelles. Small-Angle X-ray Scattering and Phase Behavior Study. *J. Chem. Phys.* **2003**, *118* (7), 3329−3333.
(30) Zhang, J.; Han, B.; Zhao, Y.; Li, W.; Liu, Y. Emulsion Inversion Induced by CO_2. *Phys. Chem. Chem. Phys.* **2011**, *13* (13), 6065−6070.
(31) Zhang, J.; Han, B.; Zhao, Y.; Li, J.; Yang, G. Switching Micellization of Pluronics in Water by CO_2. *Chem.−Eur. J.* **2011**, *17* (15), 4266−4272.
(32) Ganapathy, H. S.; Hwang, H. S.; Lee, M. Y.; Jeong, Y. T.; Gal, Y.-S.; Lim, K. T. Stabilizer Architectures Based on Fluorinated Random and Block Copolymers for the Dispersion Polymerization of 2-Hydroxyethyl Methacrylate in Supercritical Carbon Dioxide. *J. Mater. Sci.* **2008**, *43* (7), 2300−2306.
(33) Oh, K. S.; Bae, W.; Kim, H. Dispersion Polymerization of 2-Hydroxyethyl Methacrylate (HEMA) Using Siloxane-Based Surfactant in Supercritical Carbon Dioxide and in Compressed Liquid Dimethyl Ether. *Eur. Polym. J.* **2008**, *44* (2), 415−425.
(34) Alaimo, D.; Beigbeder, A.; Dubois, P.; Broze, G.; Jerome, C.; Grignard, B. Block, Random and Palm-Tree Amphiphilic Fluorinated Copolymers: Controlled Synthesis, Surface Activity and Use as Dispersion Polymerization Stabilizers. *Polym. Chem.* **2014**, *5* (18), 5273−5282.
(35) Lutz, J.-F.; Akdemir, Ö.; Hoth, A. Point by Point Comparison of Two Thermosensitive Polymers Exhibiting a Similar LCST: Is the Age of Poly(NIPAM) Over? *J. Am. Chem. Soc.* **2006**, *128* (40), 13046−13047.
(36) Glinel, K.; Jonas, A. M.; Jouenne, T.; Leprince, J.; Galas, L.; Huck, W. T. S. Antibacterial and Antifouling Polymer Brushes Incorporating Antimicrobial Peptide. *Bioconjugate Chem.* **2009**, *20* (1), 71−77.
(37) Lutz, J.-F.; Hoth, A. Preparation of Ideal PEG Analogues with a Tunable Thermosensitivity by Controlled Radical Copolymerization of 2-(2-Methoxyethoxy)ethyl Methacrylate and Oligo(ethylene glycol) Methacrylate. *Macromolecules* **2005**, *39* (2), 893−896.
(38) Roy, D.; Brooks, W. L. A.; Sumerlin, B. S. New Directions in Thermoresponsive Polymers. *Chem. Soc. Rev.* **2013**, *42* (17), 7214−7243.
(39) de las Heras Alarcon, C.; Pennadam, S.; Alexander, C. Stimuli Responsive Polymers for Biomedical Applications. *Chem. Soc. Rev.* **2005**, *34* (3), 276−285.
(40) Glatter, O.; Kratky, O., Eds. *Small Angle X-ray Scattering*; Academic Press: New York, 1982; 515 pp.
(41) Feigin, L. A.; Svergun, D. I. *Structure Analysis by Small-Angle X-ray and Neutron Scattering*; Plenum Press: New York, 1987.
(42) Pedersen, J. S. Analysis of Small-Angle Scattering Data from Colloids and Polymer Solutions: Modeling and Least-Squares Fitting. *Adv. Colloid Interface Sci.* **1997**, *70* (0), 171−210.
(43) Sivia, D. S. *Elementary Scattering Theory: For X-ray and Neutron Users*; Oxford University Press: Oxford, U.K., 2011.
(44) Gommes, C. J.; Pirard, J.-P.; Goderis, B. Condensation-Induced Decrease of Small-Angle X-ray Scattering Intensity in Gelling Silica Solutions. *J. Phys. Chem. C* **2010**, *114* (41), 17350−17357.
(45) Stryjek, R.; Vera, J. H. PRSV: An Improved Peng-Robinson Equation of State for Pure Compounds and Mixtures. *Can. J. Chem. Eng.* **1986**, *64* (2), 323−333.
(46) Bras, W.; Dolbnya, I. P.; Detollenaere, D.; van Tol, R.; Malfois, M.; Greaves, G. N.; Ryan, A. J.; Heeley, E. Recent Experiments on a Small-Angle/Wide-Angle X-ray Scattering Beam Line at the ESRF. *J. Appl. Crystallogr.* **2003**, *36* (3, Pt. 1), 791−794.
(47) Hermida-Merino, D.; Portale, G.; Fields, P.; Wilson, R.; Bassett, S. P.; Jennings, J.; Dellar, M.; Gommes, C.; Howdle, S. M.; Vrolijk, B. C. M.; et al. A High Pressure Cell for Supercritical CO_2 On-line Chemical Reactions Studied with X-ray Techniques. *Rev. Sci. Instrum.* **2014**, *85* (9), No. 093905.
(48) Huang, T. C.; Toraya, H.; Blanton, T. N.; Wu, Y. X-ray Powder Diffraction Analysis of Silver Behenate, a Possible Low-Angle Diffraction Standard. *J. Appl. Crystallogr.* **1993**, *26* (2), 180−184.
(49) Gommes, C. J.; Goderis, B. CONEX, a Program for Angular Calibration and Averaging of Two-Dimensional Powder Scattering Patterns. *J. Appl. Crystallogr.* **2010**, *43* (2), 352−355.
(50) Debye, P. Molecular-Weight Determination by Light Scattering. *J. Phys. Colloid Chem.* **1947**, *51*, 18−32.
(51) Nakano, M.; Deguchi, M.; Matsumoto, K.; Matsuoka, H.; Yamaoka, H. Self-Assembly of Poly(1,1-diethylsilabutane)-*block*-poly-

DOI: 10.1021/jp5086558
J. Phys. Chem. B 2015, 119, 1706−1716

(2-hydroxyethyl methacrylate) Block Copolymer. 1. Micelle Formation and Micelle−Unimer−Reversed Micelle Transition by Solvent Composition. *Macromolecules* **1999**, *32* (22), 7437−7443.
(52) Hammouda, B. A New Guinier-Porod Model. *J. Appl. Crystallogr.* **2010**, *43* (4), 716−719.
(53) De Gennes, P.-G. *Scaling Concepts in Polymer Physics*; Cornell University Press: Ithaca, NY, USA, 1979.
(54) Billmeyer, F. W., Jr. *Textbook of Polymer Science*, 3rd ed.; Tokyo Denki University Press: Tokyo, 1989.
(55) Pedersen, J. S.; Gerstenberg, M. C. Scattering Form Factor of Block Copolymer Micelles. *Macromolecules* **1996**, *29* (4), 1363−1365.

DOI: 10.1021/jp5086558
J. Phys. Chem. B 2015, 119, 1706−1716